AIChE WILEY InterScience DISCOVER SOMETHING GREAT

Spatial Near-Infrared Imaging of Hydroxyl Band Coverage on Ceria-Based Catalysts

Farid Aiouache, Hiro Oyama, and Kuniyuki Kitagawa
Ecotopia Science Institute, Nagoya University, Chikusa-ku 464-8603, Nagoya, Japan

DOI 10.1002/aic.10731
Published online December 6, 2005 in Wiley InterScience (www.interscience.wiley.com).

High-throughput near-infrared imaging was used to distinguish catalyst activity for low-temperature methane steam-reforming. Geminal hydroxyls of reduced ceria were depicted during methane reforming at 673 K. The changes in absorbance maps under various water partial pressures showed evidence of formate intermediate formations without redox exchanges. Higher resolution was observed in absorbance change images than that of thermal images obtained from catalyst surface self-emissions. The experimental results illustrated higher activity of pure rhodium catalyst than that of bimetallic ones, likely because of the high dispersion of rhodium on the catalyst support. Moreover, the reaction was accelerated when high surface area silica was added because more reduced sites were exposed. Our filter bandwidths limited our interest in band-shift distribution of geminal hydroxyl band during the reduction process. © 2005 American Institute of Chemical Engineers *AIChE J,* 52: 1516–1521, 2006
Keywords: near-infrared imaging, methane reforming, ceria, redox, combinatorial, high throughput

Introduction

The combination of in situ thermal images with combinatorial chemistry is receiving more attention in various microsystem applications.[1-3] High-throughput screening of "multi sample at a time" in a library by infrared radiations under spectroscopic or thermal imaging has been used to detect hot area and breathing patterns of catalytic surfaces.[4-8] However, thermographic methods remain uncertain with respect to probing weakly thermal exchanges during reaction–diffusion operations. At atmospheric pressure, Qin and Wolf[9] introduced a species-sensitive method by filtering radiations received by an infrared (IR) camera detector to spectral vibrations of CO free of passive background radiations. CO linear coverage of rhodium/silica catalyst could be observed through spatiotemporal images based on thermal and absorbance emissions. The results were most valid at low temperatures and pseudoisothermal conditions. Snively et al.[10] used Fourier transformed infrared (FTIR) imaging by coupling an FTIR spectrometer and a focal plane detector to quantitatively visualize emissions of CO_2 produced from CO oxidation using a library of 16 samples. A two-dimensional (2D) imaging based on species sensitivity was also investigated by Su and Yeung,[11] who probed vanadium pentoxide activity for naphthalene oxidation at low temperatures by using a laser-induced fluorescence source. A low fluid distortion on fluorescence-based images was observed at low temperatures, whereas a good resolution on near-infrared (NIR) thermography-based images was obtained at high temperatures. Olk et al.[12] screened hydrogen sorption on a thin film of Mg-based alloys for hydrogen storage by following apparent temperature changes related to emissivity variations of resulted hydrides.

In this work, we propose near-infrared imaging (NIRI) as an alternative mapping technique for screening atmospheric adsorption of molecules with high vibration bands in the NIR range, as opposed to individual reactants and products IR emissions. We consider bridged-bond or geminal hydroxyls (OH) overtones on reducible cerium oxide at temperatures of 673 and 823 K. We applied the results to CH_4 steam-reforming at 673 and 823 K, denoted as low and middle temperatures of CH_4 reforming, respectively. These temperatures were selected because two different processes

© 2005 American Institute of Chemical Engineers

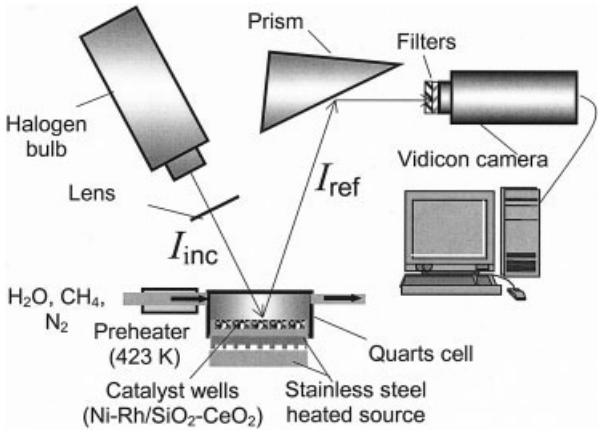

Figure 1. Experimental setup for high-throughput NIR imaging.

may prevail on catalyst surfaces. Although the redox process is well observed at middle and high temperatures by carbonate intermediate formation, it is unlikely that it occurs at low-temperature reforming because surface OH may convert chemisorbed carbonyls to formates instead of carbonates. Jacob et al.[13] reported a nonmediated ceria process for water gas shift (WGS) reaction. The observations by in situ diffuse reflectance infrared Fourier transform spectroscopy (DRIFT) of reaction rate profiles at high water to CO molar ratios and X-ray absorption near edge spectroscopy (XANES) agreed with "via formate mechanism" and without oxidation by water. In our work, selected compositions of catalyst are screened by high-throughput imaging (HTI) in a continuous multiwell reactor.

Experimental

Catalyst preparation

The catalyst was prepared by an incipient wetness method[13] using an aqueous solution of $Ce[(NH_4)_2(NO_3)_6]$ (Wako Pure Chemicals, Osaka, Japan) and SiO_2 (Aerosil, 380 m^2/g, Sigma-Aldrich, St. Louis, MO). After loading CeO_2 and SiO_2, the sample was dried at 383 K for 12 h and then was calcinated at 773 K for 3 h under oxygen atmosphere ($P_{O_2} = 1.013 \times 10^4$ Pa). Rhodium and nickel were loaded on CeO_2/SiO_2 by impregnation of the support with a solution of $Ni[(NO_3)_2{\cdot}6H_2O]$ (Chameleon Reagent, Osaka, Japan) and $Rh(C_5H_7O_2)_3$ (Aldrich Chemical, Milwaukee, WI) in ethanol (Wako Pure Chemicals). The solvent was removed by drying the catalyst at 383 K for 12 h under nitrogen atmosphere. The calcination was carried out at 773 K under oxygen atmosphere ($P_{O_2} = 10.13$ kPa).

Apparatus

The HTI experiments were carried out in a homemade quartz glass cell to allow a high transparency in the NIR range, as shown in Figure 1. The cell includes 25 wells (5 lines × 5 columns, diameter: 4×10^{-3} m). The wells were obtained on a ceramic template (diameter: 4×10^{-2} m) that was supported on a stainless steel plate. The experimental setup allowed a homogeneous heat transfer through the ceramic template. Each well contained approximately 0.021 g of the catalyst.

Analysis

The diffuse reflectance NIR was conducted with a multichannel fiber probe spectrometer equipped with InGaAs linear image sensor (Jasco, Tokyo, Japan). A lens was mounted on the probe and positioned at 10 mm from the quartz window. Because air absorption was negligible, no purging system was required. One test required 100 scans.

A Vidicon camera (Model 2701-03, Hamamatsu Photonics®, Olympus America, Melville, NY), with sensing wavelengths from 400 to 2200 nm, was used for NIR imaging. Two band-pass interference filters (Andover Corp., Salem, NH), centered at 1381 and 1369 nm, were placed in front of the lens of the camera. The images were taken under visible light with and without illumination from 50 W halogen bulbs. The experiments were carried out under temperatures that allow significant NIR emissions from samples. Then, images representing self-emissions of samples in the absence of the external illumination were subtracted to obtain images from reflected radiations. All images were captured by a frame-grabber card (CT3000) and postprocessed by commercial image-processing software.

Results

Absorbance changes under NIR light source

At high temperatures, the measured radiations received by a NIR spectrometer or a camera detector from catalyst surfaces contain gray body radiations from catalyst surface, reflected radiations issued from external illumination, and background radiation at the surrounding temperature. In the following equation, the terms I_{ref}, I_{emi}, and I_{surr} represent reflected radiations from the external source (halogen bulb), emitted radiations from the catalyst surface, and reflected radiations from the surrounding environment, respectively:

$$I_t^{ON} = I_{ref} + I_{emi} + I_{surr,1} \tag{1}$$

In the absence of external illumination, I_{ref} disappears and the measured radiations are given by

$$I_t^{OFF} = I_{emi} + I_{surr,2} \tag{2}$$

If the camera offset is adjusted to the surrounding area, absorbance change (ΔAbs) signal of surface hydroxyl density will be given by

$$\Delta Abs = \log \frac{I_t^{ON} - I_t^{OFF}}{I_{t0}^{ON} - I_{t0}^{OFF}} \tag{3}$$

Geminal hydroxyls of ceria support during hydrogen reduction and CH_4 reforming at low temperatures

Several authors discussed the mechanism of ceria reduction,[13,15] which can be represented by

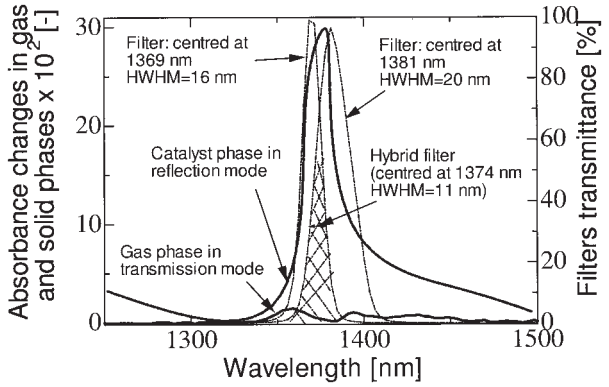

Figure 2. NIR Spectra of absorbance and transmittance profiles after 15 min of reduction at 673 K.

P_{H_2} = 10.13 kPa; feed flow rate = 1 mL/s.

$$CeO_2 + \left(y + \frac{x}{2}\right)H_2 \Rightarrow CeO_{2-x-y}(OH)_x + yH_2O \qquad (4)$$

$$CeO_2 + \frac{1}{2}H_2 \Leftrightarrow \frac{1}{2}Ce_2O_3 + \frac{1}{2}H_2O \qquad (5)$$

The irreversible reaction 4 and reversible reaction 5 reflect reduction of Ce^{4+} ions at the surface and bulky layers, respectively.

At middle temperatures, Eq. 5 leads CH_4 reforming to occur through reactions 6–9 as cited by Wei and Iglesia.[16] The authors observed that water partial pressure was noneffective on reaction rate and the activation of C–H bond in CH_4 was a limiting step, whereas the remaining reactions were quasi-equilibrated. Accordingly, the CH_4 reforming mechanism proceeds through Eqs. 6–10, where σ represents an active surface site:

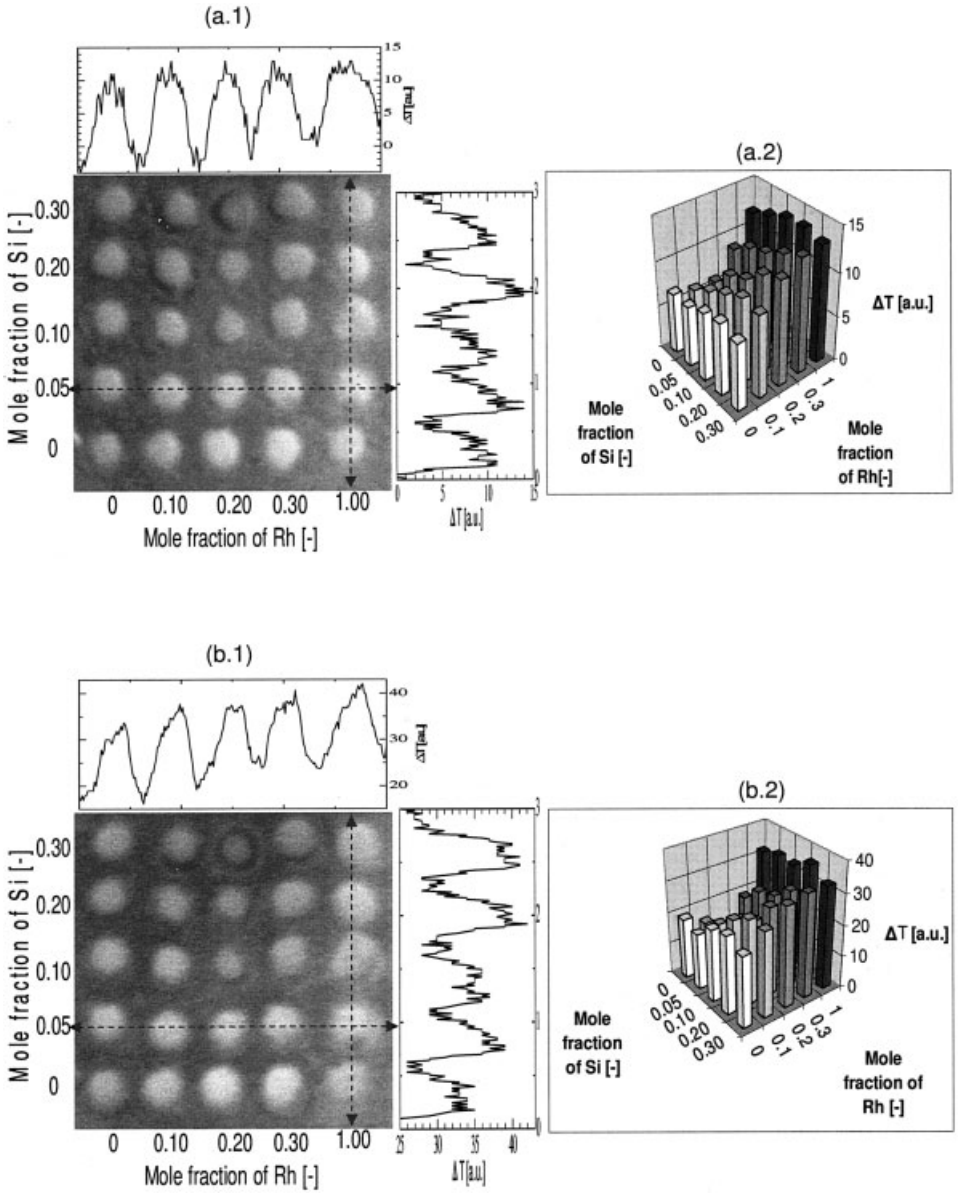

Figure 3. NIR self-emission images (a1, b1) and integrated value profiles (a2, b2) after 15 min of reduction.

P_{H_2} = 10.13 kPa; feed flow rate = 1 mL/s. (a) T = 673 K, (b) T = 823 K.

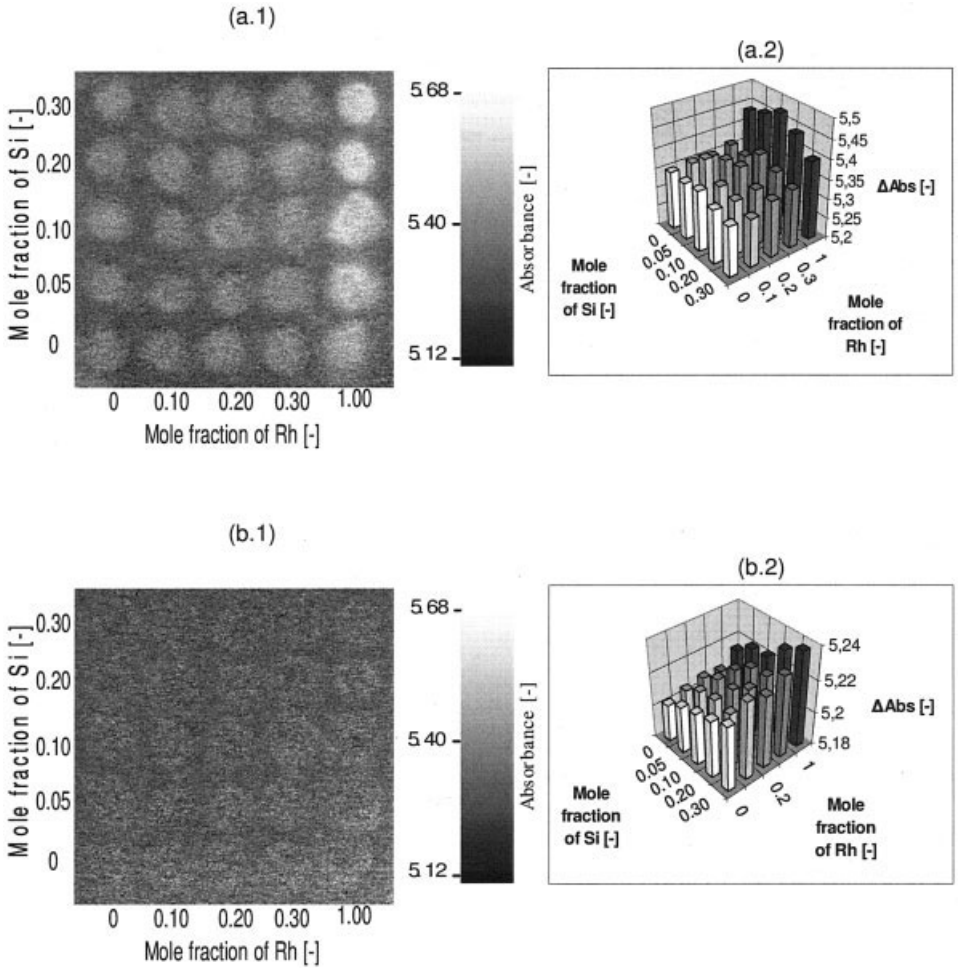

Figure 4. Absorbance change images (a1, b1) and integrated value profiles (a2, b2) after 15 min of reduction.

P_{CH_4} = 10.13 kPa; feed flow rate = 1 mL/s. (a) T = 673 K, (b) T = 823 K.

$$CH_4 + \sigma \Leftrightarrow CH_{x\sigma} + \left(\frac{4-x}{2}\right)H_2 \quad (6)$$

$$H_2O + 2\sigma \Leftrightarrow 2O\sigma + H_2 \quad (7)$$

$$CH_{x\sigma} + O_\sigma \Leftrightarrow CO\sigma + \frac{x}{2}H_2 + \sigma \quad (8)$$

$$CO_\sigma + O_\sigma \Leftrightarrow CO_2 + 2\sigma \quad (9)$$

On the other hand, the nonoxidation of ceria by water in reaction 4 at low temperatures would lead Eqs. 7–9 to proceed through the following series of equations:

$$H_2O + \sigma \Leftrightarrow H_2O\sigma \quad (10)$$

$$CH_{x\sigma} + H_2O\sigma \Leftrightarrow CO\sigma + \left(\frac{x+2}{2}\right)H_2 + \sigma \quad (11)$$

$$CO\sigma + H_2O\sigma \Leftrightarrow CO_2 + H_2 + 2\sigma \quad (12)$$

Changes in forward reaction rates of CH_4 reforming for various ratios of water/CH_4 can show evidence of a formate-relevant step at low-temperature reforming.

Geminal OH Probing by Hydrogen Reduction

Steam and OH spectral profiles by NIR spectrometer

Preliminary tests were carried out by adding hydrogen in N_2 flow (P_{H_2} = 10.13 kPa) at 673 K. Figure 2 shows gas and surface catalyst spectra of a single catalyst well with pure rhodium on ceria [Rh (1 wt %) and CeO_2 (99 wt %)] at 673 K and after 15 min of reduction time. The gas-phase spectrum was recorded in transmission mode by directing NIR illumination at 1 cm above the catalyst surface, whereas the condensed-phase spectrum was obtained in reflection mode. Spectra profiles in Figure 2 display the advantage of combining two filters with a resulting bandwidth of 11 nm to locate the OH overtone band in 2D imaging during the reduction by hydrogen. The ΔAbs in the gas phase was caused by radiations of the generated steam, whereas ΔAbs from the catalyst surface originated from the adsorbed hydroxyls in accordance with Eq. 4. The ΔAbs of the gas phase is about one twentieth of the ΔAbs

observed on catalyst surface at the wavelength range of our interest. As opposed to IR observations, OH coverage of ceria is weakly masked by gas-phase hydroxyl bands in NIR range. Although a blue shift of 8 cm^{-1} in the IR range was observed by Marco et al.,[17] it was hard to distinguish any shift of OH in NIR because of the limited pixel resolution with the spectrometer used. For instance, geminal OH bonds, close and far to oxygen vacant sites, may play different roles during CH_4 reforming because they can show different desorption temperatures.

Thermal and absorbance imaging of catalyst library

A library of 25 catalyst samples was examined under hydrogen reduction (P_{H_2} = 10.13 kPa) at two temperatures of 673 and 823 K and 15 min of reduction time. Figure 3 displays temperature changes from NIR thermal images captured before and after hydrogen addition, in the absence of the external illumination and computed from Eq. 2. The library lines and columns represent Rh and Si mole fraction variations, respectively. At 623 K, a decrease in the temperature is observed in all well surfaces, in agreement with endothermic reduction of ceria. At 823 K, temperature changes are more pronounced than those at 673 K. Accordingly, larger numbers of Ce^{4+} were reduced and probably oxygen vacancies were produced not only on the surface but also at bulk ceria layers. Thermal boundaries crossing well borders are well defined with well catalysts rich in rhodium and silica. Because the exceeding thermal transfer between wells may lead to misleading results, a correction of active surface emissivity changes by mapping ΔAbs was attempted. As displayed in Figure 4, 2D images of OH ΔAbs do not cross borders well at either temperature. Surface wells loaded with pure rhodium display significant ΔAbs values compared with those of bimetallic catalysts of nickel and rhodium. This result agrees with previous findings shown in Figure 3 and based on thermal imaging. However, ΔAbs values are less pronounced at 823 K for all wells, although corresponding temperature changes were higher than those obtained at 673 K in Figure 3. Then, the extended reduction to bulky layers of ceria was likely accompanied by surface OH elimination. On the other hand, gain nonlinearity of the Vidicon camera did not allow us to pursue a quantitative analysis between ΔAbs and retained OH accessible by gas chromatography.

Application to CH_4 Steam-reforming

The generation and extent of coverage of geminal OH bonds on ceria-promoted catalysts during low-temperature CH_4 reforming are demonstrated in Figure 5. The reduced catalysts at 823 K were exposed to CH_4 steam-reforming after decreasing the temperature to 673 K and under N_2 atmosphere. ΔAbs values of OH are linear with water vapor pressure, whereas they would be negligible if catalysts were previously exposed to water alone. Similar to the previous finding on catalyst reduction by hydrogen, the increase in ΔAbs is more pronounced for catalyst wells rich in rhodium. Because CH_4 reforming reaction at 673 K is relatively slow, a forward reaction mechanism can be investigated far from equilibrium conditions. The changes of absorbances with water to CH_4 ratios indicate reaction of formates with water as a relevant step

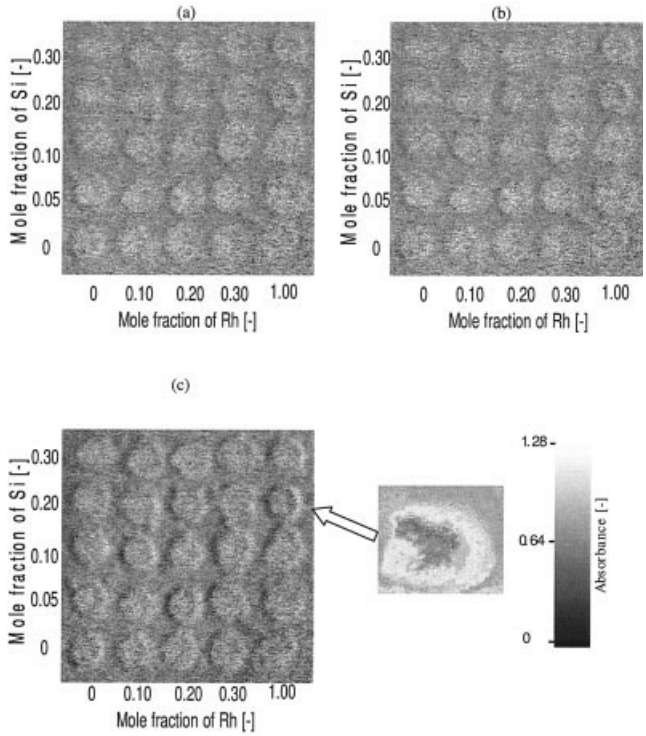

Figure 5. Absorbance rate images of catalyst surfaces (reduced at 823 K) at P_{CH_4} = 10.13 kPa.

P_{H_2O}/P_{CH_4}: (a) 1/1, (b) 2/1, (c) 5/1; feed flow rate = 1 mL/s; T = 673 K.

in the overall pathway of CH_4 reforming. Because water molecules and terminal OH on ceria desorb at temperatures < 473 K, water reacts with surface carbonyls to formate and carbonate intermediates. Ultimately, the generated formates react with water to form CO, CO_2, and H_2, as described by Eqs. 10–12. At experimental conditions, single formates or formates and carbonates could not be confirmed. However, if we add our finding to that of Jacob et al.[13] on WGS reaction at low temperatures, we may conclude that the overall reaction proceeded without redox exchanges. In addition, silica addition to ceria support was beneficial to CH_4 reforming. This positive effect of silica may be derived from potential generation of a new crystallite ceria silicate phase $Ce_{9.33}(SiO_4)_2O_2$[18] with a hexagonal rearrangement. Given this, the $Ce_{9.33}(SiO_4)_2O_2$ phase displays high surface hydroxylation with oxygen vacancy limits that were improved over those of pure ceria. On the other hand, nickel addition to rhodium was not effective because of its low surface dispersion. This finding is different from that reported in several works,[19-21] where activity of bimetallic catalysts of Rh–Ni was found unchanged or improved over that of corresponding single metals. Describing flow penetration in a well as shown in the enlarged image of Figure 5, gradient profiles of OH ΔAbs along the radial direction are clearly observed, although boundary layers of associated heat and mass transfers were minimized under a feed flow rate of 0.1 L/min (STP) and catalyst size of 0.0266 mm.

Conclusions

In this work, we attempted to depict 2D NIR imaging of geminal hydroxyls distribution on a ceria-support catalyst.

Thermal and differential absorbance modes were used in a high-throughput library for hydrogen reduction and CH_4 reforming. Absorbance-based images were more sensitive to OH ΔAbs than the thermographic images, which were limited by heat transfer exchanges between catalyst wells. Moreover, rhodium and silica satisfactorily promoted ceria activity for CH_4 reforming. This latter was found likely to proceed by formate intermediates at low temperatures and without redox process. Finally, this work will be extended to CH_4 autoreforming where heat exchange properties of complex reactions and component adsorptions will provide improved information on image resolution between those obtained from the self-emissions and the ΔAbs images.

Acknowledgments

The authors are grateful to National Energy Development Organisation (NEDO) for financial support.

Literature Cited

1. Tibiletti D, Bart de Graaf EA, Teh SP, Rothenberg G, Farrusseng D, Mirodatos C. Selective CO oxidation in the presence of hydrogen: Fast parallel screening and mechanistic studies on ceria-based catalysts. *J Catal.* 2004;225:489-497.
2. Holzwarth A, Schmidt H, Maier W. Detection of catalytic activity in combinatorial libraries of heterogeneous catalysts by IR thermography. *Angew Chem Int Ed Engl.* 1998;37:2644-2647.
3. Haap WJ, Walk TB, Jung G. FT-IR mapping—A new tool for spatially resolved characterization of polymer-bound combinatorial compound libraries with IR microscopy. *Angew Chem Int Ed Engl.* 1998;110: 3506-3509.
4. Snively CM, Oskardottir G, Lauterbach J. Parallel analysis of the reaction products from combinatorial catalyst libraries. *Angew Chem Int Ed Engl.* 2001;40:3028-3030.
5. Moates FC, Somani M, Annamalai J, Richardson JT, Luss D, Willson RC. Infrared thermographic screening of combinatorial libraries of heterogeneous catalysts. *Ind Eng Chem Res.* 1996;35:4801-4803.
6. Reetz MT, Becker MH, Kühling KM, Holzwarth A. Time-resolved IR-thermographic detection and screening of enantioselectivity in catalytic reactions. *Angew Chem Int Ed Engl.* 1998;37:2647-2650.
7. Senkan SM. High-throughput screening of solid-state catalyst libraries. *Nature.* 1998;394:350-353.
8. Taylor SJ, Morken JP. Thermographic selection of effective catalysts from an encoded polymer-bound library. *Science.* 1998;280:267-270.
9. Qin F, Wolf EE. Spatially resolved infrared spectroscopy: A novel technique for in situ study of spatial surface coverage during CO oxidation on supported catalysts. *Catal Lett.* 1996;39:19-15.
10. Snively CM, Oskarsdottir G, Lauterbach J. Chemically sensitive parallel analysis of combinatorial catalyst libraries. *Catal Today.* 2000; 67:357-368.
11. Su H, Hou Y, Houk RS, Schader GL, Yeung ES. Combinatorial screening of heterogeneous catalysts in selective oxidation of naphthalene by laser-induced fluorescence imaging. *Anal Chem.* 2001;73: 4434-4440.
12. Olk CH, Tibbetts GG, Simon D, Moleski JJ. Combinatorial preparation and infrared screening of hydrogen sorbing metal alloys. *J Appl Phys.* 2003;94:720-725.
13. Jacobs G, Patterson PM, Williams L, Sparks D, Davis BH. Low temperature water-gas shift: Role of pretreatment on formation of surface carbonates and formats. *Catal Lett.* 2004;96:97-105.
14. Asadullah M, Miyazawa T, Ito S, Kunimori K, Tomishige K. Demonstration of real biomass gasification drastically promoted by effective catalyst. *Appl Catal A: Gen.* 2003;246:103-116.
15. Montagne X, Lynch J, Freund E, Lamotte J, Lavalley AJC. Study of the adsorption sites on thoria by scanning-transmission electron-microscopy and Fourier-transform infrared-spectroscopy—Adsorption and desorption of water and methanol. *J Chem Soc Faraday Trans I.* 1987;83:1451-1459.
16. Wei J, Iglesia E. Isotopic and kinetic assessment of the mechanism of reactions of CH_4 with CO_2 or H_2O to form synthesis gas and carbon on nickel catalysts. *J Catal.* 2004;224:370-383.
17. Daturi M, Finocchio E, Binet C, Lavalley JC, Fally F, Perrichon V. Study of bulk and surface reduction by hydrogen of $CexZr1\text{-}xO_2$ mixed oxides followed by FTIR spectroscopy and magnetic balance. *J Phys Chem B.* 1999;103:4884-4891.
18. Rocchini E, Trovarelli A, Llorca J, Graham GW, Weber WH, Maciejewski M, Baiker A. Relationships between structural/morphological modifications and oxygen storage-redox behavior of silica-doped ceria. *J Catal.* 2000;194:461-478.
19. Irusta S, Cornaglia LM, Lombardo EA. Hydrogen production using Ni-Rh on ZrO_2 as potential low-temperature catalysts for membrane reactors. *J Catal.* 2002;210:263-272.
20. Hou ZY, Yashima T. Small amounts of Rh-promoted Ni catalysts for methane reforming with CO_2. *Catal Lett.* 2003;3/4:193-197.
21. Nowosielska M, Jozwiak WK, Rynkowski JM. The activity of Al_2O_3-supported bimetallic Ni-Rh catalysts in the reforming of methane with carbon dioxide. *Prez Chem.* 2003;82:744-747.

Manuscript received Apr. 19, 2005, and revision received Oct. 14, 2005.